Long-time translational self-diffusion in isotropic and nematic dispersions of colloidal rods

M. P. B. van Bruggen,[1] H. N. W. Lekkerkerker,[1] G. Maret,[2] and J. K. G. Dhont[1,*]
[1]*Van 't Hoff Laboratory for Physical and Colloid Chemistry, Debye Institute, Utrecht University, Padualaan 8, 3584 CH Utrecht, The Netherlands*
[2]*Universität Konstanz, Fakultät für Physik, P.O. Box 5560, D-78434 Konstanz, Germany*
(Received 27 April 1998)

Long-time self-diffusion in dispersions of rigid colloidal rods with an aspect ratio of 19 is studied with fluorescence recovery after photobleaching (FRAP) in isotropic and nematic phases. The long-time self-diffusion coefficient D_s^L is found to decrease linearly with concentration up to $(L/D)\phi=0.12$ (with L the length and D the diameter of the rods, and ϕ the volume fraction). In the isotropic phase in coexistence with the nematic phase, D_s^L remains virtually constant at about 1% of its value at infinite dilution. In the nematic phase long-time self-diffusion is found to be ten times slower than in the coexisting isotropic phase. In addition, by modifying the FRAP geometry we were able to distinguish between sidewise and lengthwise diffusion in aligned nematic phases. [S1063-651X(98)11712-9]

PACS number(s): 82.70.Dd, 83.10.Pp, 83.70.Jr

I. INTRODUCTION

Large differences in both dynamics and phase behavior of rodlike particles and macromolecules can evolve at low volume fractions when the rods are long and thin. In this paper we study the long-time dynamics of *individual* rods interacting with other rods, a property called long-time *self*-diffusion.

Self-diffusion can be studied by dynamic light scattering (DLS), but for this one needs tracer systems, which are difficult to prepare. In addition it is not trivial to extract true long-time results from DLS data. More suitable techniques for studying long-time self-diffusion are forced Rayleigh scattering (FRS) and fluorescence recovery after photobleaching (FRAP). Both techniques require particles that are labeled with an appropriate photosensitive dye. Wang, Garner, and Yu [1] performed FRS experiments with short DNA fragments (150 base pairs in length) whereas Bu *et al.* [2] performed FRAP measurements on PBLG polymers of various molecular weights. In addition self-diffusion properties of phage λ DNA with lengths of about 50 000 base pairs were studied by Scalettar, Hearst, and Klein [3]. All polymers used in these studies are to a certain extent flexible. van Bruggen, Lekkerkerker, and Dhont [4] used inorganic colloidal silica (SiO_2) rods as a model system for truly *rigid* rods. Their data show an extended linear dependence between the long-time self-diffusion coefficient and concentration. In the other studies mentioned, a concentration *in*dependence at low polymer concentrations [2] and an exponential decay of the long-time self-diffusion coefficient [1] was found, indicating that flexibility strongly affects the self-diffusive behavior of rodlike particles.

In this paper, we describe the preparation of a dispersion consisting of rigid fluorescent colloidal boehmite (AlOOH) rods of which the concentration dependence of the long-time self-diffusion coefficient is measured with FRAP. Compared to the silica rod dispersion used in our earlier study [4], the aspect ratio of the boehmite rods is almost three times larger. In addition the double-layer repulsion is longer ranged in the current dispersion. These differences have a distinct effect on the physical properties of the dispersion. The boehmite dispersion separates into an isotropic and a liquid crystalline nematic phase at a high enough rod volume fraction. In the nematic phase the rods are orientationally ordered and their mean orientation is characterized by the director. The degree of alignment of the rods around the director is quantified by the orientational order parameter. A theoretical explanation for this phase transition was first given by Onsager [5].

Lateral-diffusion measurements of phospholipids in multilamellar liquid crystalline and large bilayer vesicles have been reported in the literature [6,7]. In addition fluorescence microscopy has been used for studying diffusion in nematic solutions of semiflexible *F*-actine filaments [8]. However, to our knowledge long-time self-diffusion measurements in liquid crystalline solutions of *rigid, colloidal* rods have never been reported in the literature. With the colloidal system used in this study we were able to measure diffusion coefficients in both the isotropic phase and the nematic phase. In addition diffusion along and perpendicular to the nematic director could be distinguished by proper adaptations of the geometry of the FRAP setup.

The outline of this paper is as follows. In Sec. II the preparation and modification of the colloidal system under investigation is presented and details of the experimental setups are given. In Sec. III relevant theoretical predictions are presented. In Sec. IV the results on both the characterization of the colloidal system as well as on the diffusion data are presented and discussed. Section V finishes with a summary.

II. MATERIALS AND METHODS

A. Colloidal system

1. Boehmite rods

The system used in this study consists of inorganic boehmite (AlOOH) rods dispersed in water. Boehmite rods were prepared according to the procedure of Buining *et al.* [9]. To

*Author to whom correspondence should be addressed.

2 l demineralized water, 32.0 g aluminum-tri-iso-propoxide (AIP 98%, Janssen chemica) and 40.2 g aluminum-tri-sec-butoxide (ASB, Fluka chemica) were added and the turbid mixture was stirred in a closed vessel for seven days. After autoclavation for 22 h at 150 °C and 4 bar, the resulting boehmite sol was dialyzed against flowing demineralized water for seven days. At neutral pH the rods are positively charged and are stable at low ionic strength. At concentrations of (1-1) electrolyte of the order of 10^{-2} M the rods rapidly form gels.

To protect the rods against gelation at conditions where double layer repulsion is small, a polyaluminum oxyhydroxide coating is adsorbed onto the boehmite rod surfaces. This polyaluminum oxyhydroxide is formed *in situ* by adding $Al_2(OH)_5Cl\ 2\text{-}3H_2O$, aluminum chlorohydrate (ACH), to the aqueous boehmite sol. The ability of this inorganic grafting to protect rods against gelation by screening van der Waals attraction is evidenced by the strong increase of the minimum concentration of (1-1) electrolyte necessary to gel the dispersion [10], which concentration is referred to as the critical gel concentration (cgc). To the boehmite dispersion, 0.5 mass % ACH (Locron *p*, Hoechst) was added as a powder and after 1 min of gently shaking the system was left equilibrating for three days. This dispersion will be referred to hereafter as BACH (Boehmite-ACH). The cgc of the sol has then leveled off to its maximum value. The pH of the dispersion after the addition of ACH dropped to 4–4.5. ACH solutions at this pH are known to form $Al_{13}O_4(OH)_{24}(H_2O)_{12}{}^{7+}$ polycations [11–13], further abbreviated as Al_{13}, which have a strong affinity for oxidic surfaces [14].

2. Fluorescent labeling

The stabilized rods were subsequently labeled with fluorescein isothiocyanate (FITC) in order to make them suitable for FRAP measurements. The FITC labeling was performed by preparing a solution of 52.1 mg FITC (Isomer I, Sigma) in 1.6 g ethanol (99.8% purity). Subsequently 5.6 mg of this mixture was added to 40 ml of a BACH dispersion ($c \approx 8$ g/l) and the sodium chloride concentration was then adjusted to 0.01 M NaCl. The yellowish sol was centrifuged at 2500 rpm for two days to separate the rods from free FITC molecules and ACH residual. The sediment was easily redispersed in a 0.01 NaCl stock solution. This fluorescent system is coded as $BACH^F$. Since the sediment still contains nonadsorbed ionic species, the ionic strength in the system will slightly change upon dilution. However, the Al_{13} concentration will never be larger than 3 mM, which is the total amount added. Furthermore, after removal of the free ACH, desorption of grafting material might occur to reestablish the ACH-boehmite adsorption equilibrium. Part of the negatively charged dye molecules (FITC contains one carboxylic acid group) will be connected to the positively charged ACH grafting, and therefore desorption will be accompanied by a loss of dye molecules. The extent of desorption was tested by sedimenting a $BACH^F$ dispersion that had aged for one month. The resulting supernatant was clear whereas the sediment that contained the rods was strongly yellow colored. Apparently desorption of dye molecules, and thus ACH species, is insignificant over this period of time.

B. Diffusion measurements

1. Dynamic light scattering

The translational diffusion coefficient D_0 in the limit of infinite dilution was measured with DLS. In a DLS experiment one measures, as a function of the scattering angle θ, the intensity autocorrelation function (IACF). The decay of the IACF contains information about both translational and rotational diffusivity of the rods. However, for $KL<5$ rotational contributions may be neglected and the decay of the normalized IACF $\hat{g}_I(K,t)$ is described by [15]

$$\hat{g}_I(K,t) \approx 1 + \exp(-2K^2 D_0 t), \quad KL<5, \tag{2.1}$$

with the wave vector **K** equal to

$$K = \frac{4\pi n_m}{\lambda} \sin\left(\frac{\theta}{2}\right), \tag{2.2}$$

where n_m is the refractive index of the dispersion medium and λ the wavelength of the laser in vacuo. A krypton laser (Spectra Physics 2020) was used that operates at a wavelength of 647.1 nm. The dye molecules on the rods hardly absorb light at this wavelength so that heating effects are absent. This was checked by performing the measurements on a sample with a volume fraction of 0.05% in 0.01 M NaCl at two different laser intensities yielding the same results. The IACF's were fitted to a function that included effects of polydispersity: $\hat{g}_I(K,t) = a_1 + a_2 \exp[-b(K)t + c(K)t^2]$, with $b(K)$ the decay exponent and $c(K)$ the second cumulant.

2. Fluorescence recovery after photobleaching

Technical details of the FRAP apparatus used in this study can be found in Refs. [16–19]. The wavelength of the Argon-ion laser (Spectra Physics 2000) was 488 nm and the ratio between reading intensity I_r and bleaching intensity I_b was about 10^{-3}. During the reading, it was checked that no bleaching occurred by monitoring the total fluorescent intensity directly after bleaching. The bleach pulse had a duration of 500 ms, which is small compared to the total measuring time, which varied from 1 to 20 min. The wavelength $2\pi/K$ of the sinusoidal fringe pattern (fringe spacing) was varied by varying the angle θ under which the two interfering laser beams intersect. The wave vector K is related to this angle as

$$K = \frac{4\pi}{\lambda} \sin\left(\frac{\theta}{2}\right), \tag{2.3}$$

with $\lambda = 488$ nm. Fringe spacings varied from 20 μm for the lowest concentrations to 6 μm for the highest. The fringe spacing was always much larger than the length of the rods, a condition that should be satisfied in order to ensure that long-time diffusion is monitored. Due to diffusion the amplitude $S(t)$ of the fringe pattern decreases according to [4,19]

$$S(t) \propto \exp(-D_s^L K^2 t), \tag{2.4}$$

whereas the fringe spacing remains unchanged. In FRAP one measures the temporal decay of this amplitude. The decay should be monoexponential for a genuine self-diffusion process. All decay curves were fitted to a single exponential

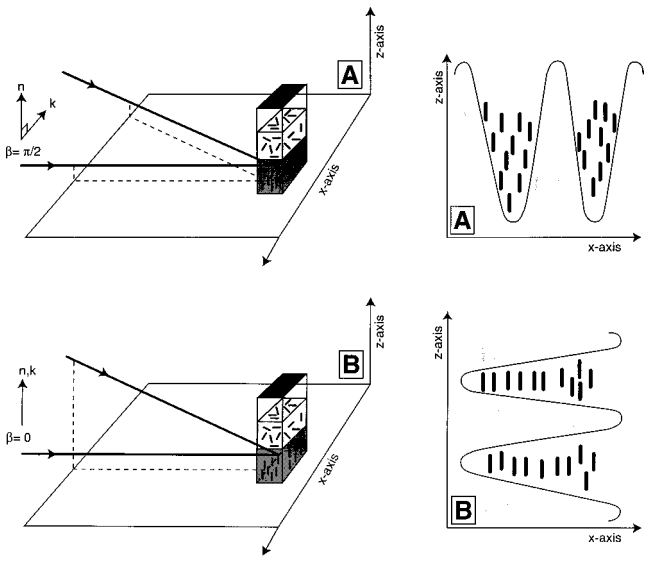

FIG. 1. Schematic drawing of the FRAP geometry. *A*: the laser beams are parallel to the ground plane and the wave vector of the fringe pattern is perpendicular on the nematic director. *B*: the beams are in a plane perpendicular on the ground plane, yielding a fringe pattern with a wave vector virtually parallel to the nematic director. The sinusoidal curves give the fluorescent intensity as a function of the x coordinate. In *A*, $D^L_{s,\perp}$ is monitored whereas in *B*, $D^L_{s,\parallel}$ is monitored.

$\sim \exp[-\alpha(K)t]$ where $\alpha(K)$ is equal to $K^2 D_s^L$ with D_s^L the long-time self-diffusion coefficient, which is the quantity of interest.

Let β denote the angle between the director of the nematic ordering **n** and the wave vector **k** of the fringe pattern. In the current FRAP setup we were able to measure at angles $\beta = 0$ as well as at $\beta = \pi/2$. For $\beta = 0$ decay of the FRAP signal is due to diffusion parallel to the nematic director whereas for $\beta = \pi/2$, diffusion perpendicular to the director causes the FRAP signal to decay. The cuvette was placed in a vertical position, so that **n** always pointed vertically. In order to change β the main laser beam was split with a beam splitter into either a horizontal or a vertical beam, perpendicular on the horizontally passing main beam, as depicted in Figs. 1(a) and 1(b), respectively. The split beam was then reflected by a piezomodulated mirror and intersected with the main beam in the sample, giving rise to the mentioned sinusoidal fringe pattern.

III. THEORY OF TRANSLATIONAL DIFFUSION

A. Translational diffusion in the limit of infinite dilution

The translational diffusion coefficient D of a Brownian rod in the isotropic phase is the orientational average of the diffusion coefficients along ($D_\parallel$) and perpendicular ($D_\perp$) to the rod's long axis, assuming that local orientational correlations are absent:

$$D = \tfrac{1}{3} D_\parallel + \tfrac{2}{3} D_\perp , \tag{3.1}$$

In the limit of infinite dilution the rods move without interacting with other rods and only experience hydrodynamic friction with the solvent. In this case D, now denoted as D_0, is given by [20]

$$D_0 = \frac{k_B T}{3\pi\eta_m L}\left[\ln\left(\frac{L}{D}\right) + 0.316 + 0.583\frac{D}{L} + 0.050\left(\frac{D}{L}\right)^2\right] \quad (\phi \to 0) \tag{3.2}$$

with η_m the viscosity of the solvent, L the length of the rod, and D its diameter, k_B Boltzmann's constant and T the absolute temperature. The last three terms within the square brackets are corrections to take Stokes friction of the segments and end effects into account.

B. Translational diffusion at higher concentrations

At increasing concentrations, the rods will start interacting and Eq. (3.2) is not applicable anymore. For hard *spherical* particles, expressions [21,22] are derived, which give the first-order concentration dependence of the long-time translational self-diffusion coefficient D_s^L, and which describe experimental the data very well [18,19]. An expression for the concentration dependence of D_s^L for rods with finite aspect ratios in the dilute regime $\{[\phi < (D/L)^2]$, with ϕ the volume fraction$\}$ is still lacking. Expressions for the concentration dependence of D_s^L at higher concentrations that have been derived for rodlike particles always separate the concentration dependence of $D_\parallel$ from $D_\perp$. At semidilute concentrations $[(D/L)^2 < \phi < D/L]$ one assumes that $D_\parallel$ is not affected by interactions, that is, $D_\parallel = D_{0,\parallel}$ with $D_{0,\parallel}$ the lengthwise diffusion coefficient at infinite dilution, whereas at higher concentrations ($\phi > D/L$) it is assumed that $D_\perp = 0$. These assumptions may be reasonable for very long and thin rodlike polymers but fail for particles with only moderate aspect ratios because then the concentration dependence of $D_\parallel$ and $D_\perp$ become more and more alike. Sato and Teramoto [23] calculated $D_\parallel$ as a function of ϕ at volume fractions around D/L assuming that diffusion takes place in tubes [24], implying that $D_\perp = 0$. By applying the same mathematical formalism, Teraoka and Hayakawa [25] calculated the concentration dependence of $D_\perp$. Combining these expressions and orientationally averaging according to Eq. (3.1), where it is assumed that local orientational correlations are absent, $D_s^L(\phi)$ becomes

$$\frac{D_s^L(\phi)}{D_0} = \frac{\frac{2}{3}D_{0,\perp}}{D_0}\left[1 + \gamma^{-1/2} 4\pi^{-1}\left(\frac{L}{D}\right)^2 \phi\right]^{-2} + \frac{\frac{1}{3}D_{0,\parallel}}{D_0}\left[1 \otimes \alpha^{-1} 4\pi^{-1}\left(\frac{L}{D}\right)^2 \phi\right]^2, \phi \approx D/L \tag{3.3}$$

with $D_{0,\perp}$ the sidewise diffusion coefficient at infinite dilution. By comparing their theory with experimental data according to Sato and Teramoto [23], α has a universal value of 13 ± 2. The factor $\gamma^{-1/2}$ in Eq. (3.3) is not known. The prefactors $\frac{2}{3}\ D_{0,\perp}/D_0$ and $\frac{1}{3}\ D_{0,\parallel}/D_0$ become equal to $\frac{1}{2}$ for high aspect ratio rods. For moderate aspect ratios the expressions of Tirado, Martinez, and de la Torre [20] for $D_{0,\perp}$ and $D_{0,\parallel}$ should be used although the validity of Eq. (3.3) for small aspect ratios is questionable since entanglement is essential in the theoretical approaches underlying Eq. (3.3). Moreover, Eq. (3.3) exhibits a minimum at higher volume

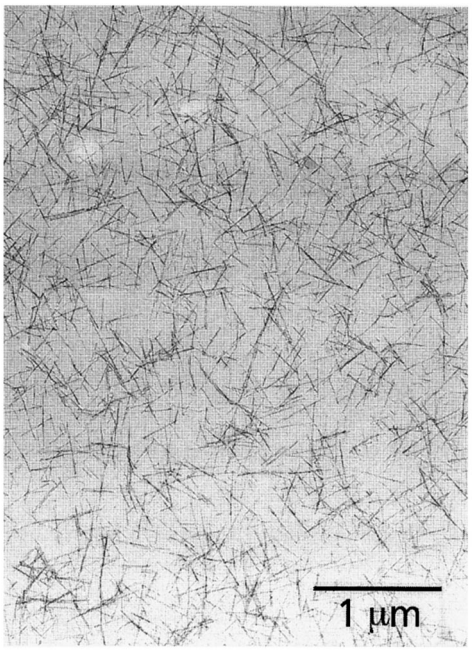

FIG. 2. Transmission electron micrograph of aluminum chlorohydrate stabilized boehmite rods which are fluorescently labeled with fluorescein isothiocyanate. The dispersion is coded as BACH^F. The ACH coating is invisible on this micrograph due to its low contrast.

fractions that is definitely unphysical. Note that the concentration of rods appears as $4\pi^{-1}(L/D)^2\phi$ in Eq. (3.3). This is equal to the number of rods in a volume L^3 and is only moderately dependent on the salt concentration when the rods are long compared to the Debye length.

The difference in both the concentration and the orientational order parameter between the isotropic and nematic phases will alter the diffusivity of the rods in these phases. Due to the orientational correlations in the nematic phase the orientational average of D_s^L as given by Eq. (3.1) does not hold anymore. As far as we know there is no theory dealing with this matter. One can reason that, on the one hand, due to the alignment of the rods the excluded volume decreases, which enhances translational diffusion. On the other hand, the higher concentration in the nematic phase will tend to decrease translational diffusion. How D_s^L will be altered in the nematic phase compared to the isotropic phase depends on the balance between these two opposing effects.

IV. RESULTS AND DISCUSSION

A. Colloidal system

1. Transmission electron microscopy (TEM) and image analysis

A TEM micrograph (Philips, CM10) of the BACH^F system *after* centrifugation and redispersion is shown in Fig. 2.

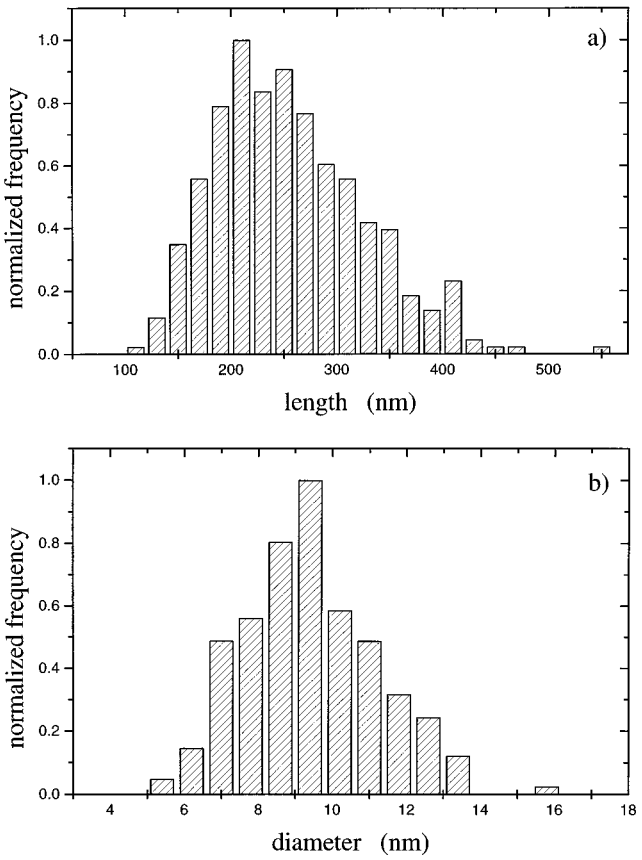

FIG. 3. (a) Length distribution of BACH^F as determined by image analysis. (b) Diameter distribution of BACH^F as determined by image analysis.

Samples were prepared by dipping copper grids coated with formvar into a very dilute aqueous boehmite dispersion to which 50% ethanol was added to promote spreading of the solvent on the hydrophobic formvar. From the TEM micrographs the average length L and average diameter D were determined with the help of an interactive image analysis system. The length and width distributions are given in Figs. 3(a) and 3(b) and the average dimensions are collected in Table I.

2. Correcting the size of the rods for the ACH-grafting and the double-layer thickness

The amount of aluminum present in the supernatant of a centrifuged BACH dispersion was determined by atomic absorption spectroscopy (AAS). From this the amount of aluminum adsorbed onto the rods was calculated, which was found to be 34 mg Al per gram of rods. The dimensions of the rods obtained with TEM should be corrected for the increased volume of the rods due to the grafting of ACH, since the low-contrast ACH grafting is invisible on the TEM mi-

TABLE I. Average dimensions of the BACH^F rods determined with TEM.

System	Length (nm)	Rel. stand. dev. (%)	Diameter (nm)	Rel. stand. dev. (%)	L/D[a]	$(L/D)_{\text{eff}}$
BACH^F	257	28	9.4	19	19	7.3

[a]L/D is the aspect ratio of the boehmite rods corrected for the adsorbed ACH-layer thickness [see Eq. (4.3)].

crographs. In view of the equilibrium composition of ACH at pH 4–4.5 [11] the adsorbed aluminum will be present in the Al_{13} form on the boehmite surfaces. Using the specific density $\rho_{Al_{13}}$ of an Al_{13} unit, which is 2.4×10^5 g/m^3 [13], and the specific surface A of these boehmite needles of 200 m^2/g [26,27], the coating thickness δ is found to be equal to

$$\delta=\frac{mM_{Al_{13}}}{13M_{Al}\rho_{Al_{13}}}\approx 2.1\ \text{nm}, \tag{4.1}$$

with $M_{Al_{13}}$ and M_{Al} the molar weights of Al_{13} (1040 g/mol) and aluminum (27 g/mol), respectively, and m the adsorbed amount of aluminum. The corrected volume fraction ϕ of the rods is then calculated by

$$\phi=\frac{v_r}{v_{r,\text{bare}}}\phi_{\text{bare}}=\frac{(L_{\text{bare}}+2\delta)(D_{\text{bare}}+2\delta)^2}{L_{\text{bare}}D_{\text{bare}}^2}\phi_{\text{bare}}=2.1\phi_{\text{bare}}, \tag{4,2}$$

with L_{bare} and D_{bare} understood to represent the average length and diameter, respectively, as determined with transmission electron microscopy, and where ϕ_{bare} is the volume fraction of bare boehmite rods with volume $v_{r,\text{bare}}$ and v_r the volume of the rods with the Al_{13} grafting. In the following, all volume fractions of BACH^F dispersions are corrected for the presence of adsorbed Al_{13}. The corrected aspect ratio is now equal to

$$\frac{L}{D}=\frac{L_{\text{bare}}+2\delta}{D_{\text{bare}}+2\delta}\approx 19, \tag{4.3}$$

where L and D represent the length and diameter of the Al_{13} grafted rods, respectively. In addition the charge on the rods also leads to an effective increase of the size of the rods. Effective hard-core dimensions are introduced by noting that rods can approach each other until their double-layer repulsion has become of the order of 1 k_BT. This procedure leads to an expression of the effective hard-core diameter D_{eff}, which is given by [4]

$$D_{\text{eff}}=D+\kappa^{-1}\ln\left[64(\tfrac{1}{2}\pi)^{1/2}cN_{\text{av}}\tanh^2\left(\frac{F|\varphi_0|}{4RT}\right)D^{1/2}L\kappa^{-(3/2)}\right] \tag{4.4}$$

with c the molar salt concentration (per m^3), N_{av} Avogadro's constant, and $|\varphi_0|$ the absolute surface potential (77.8 mV Ref. [26]), F Faraday's constant and κ^{-1} the Debye length in 0.01 M NaCl, which is 3.0 nm. In the BACH^F dispersion D_{eff} is then found to be 35.8 nm. Consequently the (corrected) aspect ratio changes into an effective hard-core aspect ratio $(L/D)_{\text{eff}}$, which in 0.01 M NaCl is given by

$$\left(\frac{L}{D}\right)_{\text{eff}}\equiv\frac{L+2\delta}{D+2\delta+7.4\kappa^{-1}}\approx 7.3, \tag{4.5}$$

Only the diameter is corrected for double-layer repulsion since the double-layer repulsion between two rods in a head-to-tail conformation is much smaller compared to the repulsion between parallel rods at the same surface-to-surface distance. Accordingly the effective hard-core volume fraction ϕ_{eff} becomes

$$\phi_{\text{eff}}=\left(\frac{D_{\text{eff}}}{D}\right)^2\phi=7.0\phi. \tag{4.6}$$

The effective hard-core aspect ratio and effective hard-core volume fraction will be used in Sec. IV B 2 where the FRAP data are compared to computer simulations on hard rods.

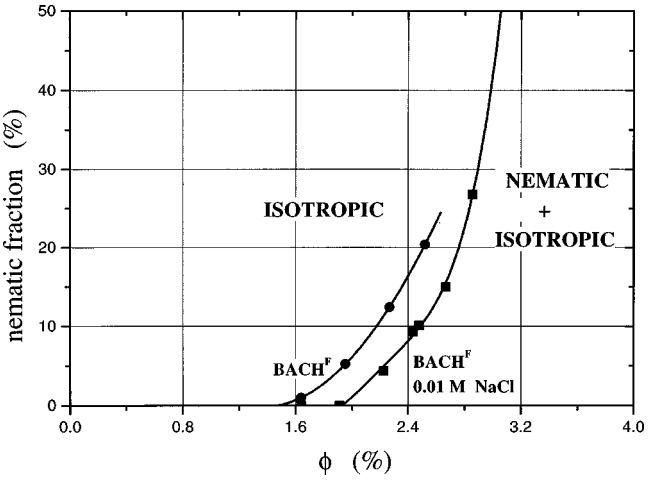

FIG. 4. The change of the nematic fraction (volume nematic phase/total dispersion volume) as a function of the overall volume fraction ϕ for BACH^F dispersions without added NaCl (●) and with 0.01 M NaCl (■). The solid lines are polynomial fits. The nonlinear increase of the nematic fraction is caused by the polydispersity of the boehmite rods. Addition of NaCl to the dispersion leads to a shift of ϕ_I to higher volume fractions. From a polynomial fit, ϕ_I and ϕ_N for the dispersion with 0.01 M NaCl (which was used in this FRAP study) were estimated as 1.9 and 3.3 %, respectively.

3. Stability and phase behavior

The ACH grafting increases the cgc from 0.05 to 0.2 M KCl [10] in boehmite dispersions with a volume fraction of 0.3%. The surface potential ϕ_0 increases only slightly from +70 to +78 mV, which cannot explain this enormously increased stability. The enhanced stability is mainly attributed to the fact that the surface charge on the rods is effectively situated at a distance equal to the ACH grafting thickness δ from the boehmite surface, while in addition the ACH layer contains a considerable amount of hydration water, making the van der Waals attraction between these layers negligible [10].

Contrary to the boehmite dispersion without ACH [26], the BACH^F dispersion quickly separates into a nematic *(N)* and an isotropic *(I)* phase when a threshold concentration ϕ_I is reached. Figure 4 shows that the boundaries of the biphasic region of a sample with 0.01 M NaCl are situated between $\phi_I=1.9\%$ and $\phi_N=3.3\%$. Here ϕ_N was estimated by fitting the relative nematic fraction versus the volume fraction with a fourth-order polynomial. For a BACH^F sample without added salt, ϕ_I shifts to 1.5%. This can be explained by the larger excluded volume of a rod at lower ionic strength that drives ϕ_I to lower values [5,28]. Figure 5 shows a polarization micrograph between crossed polarizers of the

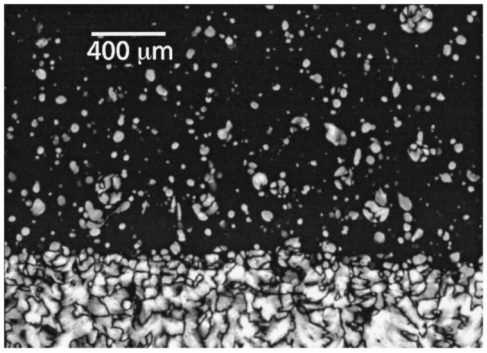

FIG. 5. Polarization light micrograph of a phase separating BACH^F dispersion with 0.01 M NaCl between crossed (north-south and east-west) polarizers. The bar represents 400 μm. The upper part is the isotropic phase containing droplets of nematic phase that sediment under gravity and finally coalesce on the bottom to form a nematic phase of macroscopic extent. Because of the alignment of the birefringent rods in the nematic droplets the polarization direction of the incident light is changed and the droplets appear as bright or dark, depending on the orientation of the rods with respect to the polarizer.

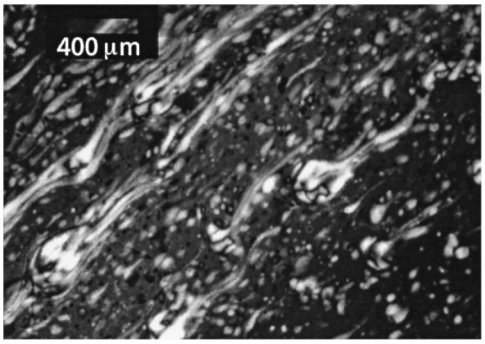

FIG. 6. Polarization light micrograph between crossed (north-south and east-west) polarizers of a phase separating dispersion of fluorescent boehmite rods while spun down at 500 rpm. The bar represents 400 μm. The picture is taken directly after switching off the centrifuge. The centrifugal force acts under an angle of 45° downwards. The largest tactoids are strongly deformed in this direction due to shear forces operating on these tactoids. The boehmite rods inside the tactoids point in the direction of the centrifugal force. The smaller tactoids are clearly much less deformed by the centrifugal action.

interface between the birefringent nematic (lower) phase and the isotropic (upper) phase, the latter of which still contains nematic droplets that ''rain out'' under gravity from the isotropic phase. These droplets (tactoids) contain the equilibrium nematic phase and ultimately coalesce to form a nematic phase of macroscopic extent on the bottom of the tube. The phase that is formed in this way shows dislocations in the director of the nematic phase. In Fig. 5 these line dislocations appear as black zones, separating the bright birefringent regions. The position of these black zones continuously changes when the object table of the polarization microscope is rotated. Apparently the director of the nematic phase is continuously spatially distributed. Because for the FRAP measurements in the nematic phase it is necessary to have a single-domain nematic phase, the next paragraph describes a technique to globally align the nematic phase.

4. Single-domain nematic phases

BACH^F dispersions of known volume and volume fraction boehmite were sedimented and the sediments were redispersed with 0.01 M NaCl up to a certain volume. These BACH^F samples were transferred to 100-μm-thick cuvettes (Vitrodynamics Inc.) with a flat bottom so that coexisting volumes of the isotropic and nematic phase could be measured conveniently from their height. Single-domain nematic BACH^F phases with a globally uniform director were obtained by centrifuging phase separating samples in 100-μm cuvettes at 500 rpm ($\sim$40 g). The tactoids which have a higher average density than the coexisting isotropic phase sediment to the bottom of the cuvette and are elongated in the direction of the centrifugal force. This is shown in Fig. 6, where the centrifugal force is directed from the right top to the left bottom corner of the figure.

The orientation of the rods in the elongated tactoids was determined as follows. A phase containing large tactoids was tilted in order to let the tactoids slide over the glass wall of the cuvette. This was done for a short period of time to prevent shear melting. Due to the large shear forces induced in this way, the tactoids are elongated into thin threads containing rods pointing in the direction of the flow. Having fixed the orientation of the rods in this way, a λ platelet (550-nm path difference) was inserted in between the sample and the analyzer, and the object stage was rotated. If the rods orientation coincided with the direction of largest refractive index of the λ platelet (commonly denoted by γ), the nematic threads appeared blue whereas after rotating over an angle $\pi/2$ they appeared orange. This proves that the direction of *largest* refractive index is along the rod *long* axis and the direction of *smallest* refractive index is along the rod *short* axis. The elongated tactoids in the centrifuged samples also appeared blue when placed parallel to γ. Apparently, even for these low shear forces, there is a strong tendency of the rods inside the tactoids to collectively align in the direction of the centrifugal force. The elongated tactoids coalesce on the bottom of the cuvette and because of their *extrinsic* (parallel elongated tactoids) as well as *intrinsic* (parallel rods inside the tactoids) orientational order, a single-domain nematic phase is formed with the director parallel to the centrifugal force. This process is completed within 48 h. The single-domain nematic phase was recognized as such by the almost total disappearance of the birefringence when the object stage of the polarization microscope (crossed polarizers) was rotated and the director of the nematic was made parallel to either the polarizer or analyzer. Whether indeed a mononematic is formed, strongly depends on the strength of the applied centrifugal force. For example, under gravity the tactoids are only slightly elongated and the tactoids organize themselves into a ''polycrystalline'' nematic phase with line dislocations, whereas at spin frequencies of 10^3 rpm the tactoids melt due to the shear forces that become increasingly stronger. The aligned nematics slowly rearranged in time. The appearance of dislocations was followed by polarization microscopy and revealed that reorganizations on a μm scale took place on a time scale of hours. As will become clear later, the self-diffusion processes in the nematic phase is typically two orders of magnitude faster than the formation of director dislocations. The slow formation of dislocations

will therefore not affect the FRAP measurements.

5. Calculating the order parameter from polarization microscopy

With a λ platelet the color of the single-nematic phase changed from bluish ($\mathbf{n}\| \gamma$) to yellow-orange ($\mathbf{n}\perp \gamma$) as the objective stage was rotated over an angle of $\pi/2$ and became deep blue again rotating $\pi/2$ further. A blue color corresponds to a total path difference of 700 nm (Ref. [29]) whereas a yellow-orange color corresponds to a path difference of 400 nm. In the first case the total pathway has increased by 150 nm whereas in the latter case it has decreased by 150 nm. From these data the order parameter of the nematic phase can be estimated. The order parameter $\langle P_2 \rangle$ can be defined as [30]

$$\langle P_2 \rangle = \frac{\Delta\varepsilon}{\Delta\varepsilon_0} \approx \frac{\Delta n}{\Delta n_0}, \tag{4.7}$$

with $\Delta\varepsilon_0$ the difference $(\varepsilon_\| - \varepsilon_0)$ of the dielectric constant within a particle and $\Delta\varepsilon$ the measured anisotropy of the dielectric constant. The refractive index n is equal to $\sqrt{\varepsilon}$. The optical pathway difference G_d between the two optical axes of the dispersion can thus be written as

$$G_d = \phi D \Delta n_0 \langle P_2 \rangle, \tag{4.8}$$

where ϕ is the volume fraction of the rods and D the thickness of the cuvette. The refractive index difference of the rod consists of two parts: the intrinsic contribution, which is about 0.01 for boehmite rods [31], and the form contribution, which has its origin in the fact that the scattered light produced by rodlike colloidal particles has a different polarization direction than the incident beam. This effect becomes very significant in dispersions of highly anisometric particles that are far from being index matched. The form effect always enhances the refractive index $n_\|$ parallel to the rod axis. Peterlin and Stuart [32] calculated the dielectric tensor of a system of perfectly aligned colloidal rods with a uniform length which is smaller than the wavelength of the incident light and when the volume fraction of the rods is low (no multiple scattering between distinct rods). For large aspect ratios, a small intrinsic inhomogeneity and a not too large index mismatch, their result can be approximated by

$$\Delta n \approx \Delta n_i + \frac{n_s^2}{4\overline{n}}\left(1 - \frac{\overline{n^2}}{n_s^2}\right)^2, \tag{4.9}$$

where Δn_i is the difference of the refractive index along the rods axis $n_\|$ and perpendicular to the rods axis $n_\perp$, and where n_m is the refractive index of the solvent and $\overline{n}$ is the average refractive index of the rods $\frac{1}{2}(n_\| + n_\perp)$. For boehmite rods dispersed in water Eq. (4.9) yields 0.10. Using the estimated volume fraction of rods in the nematic phase, corresponding to a boehmite volume fraction of 1.6%, Eq. (4.8) yields a value for $\langle P_2 \rangle$ of 0.94. This indicates that the mononematics obtained by the procedure as described in Sec. IV A 4 are highly ordered.

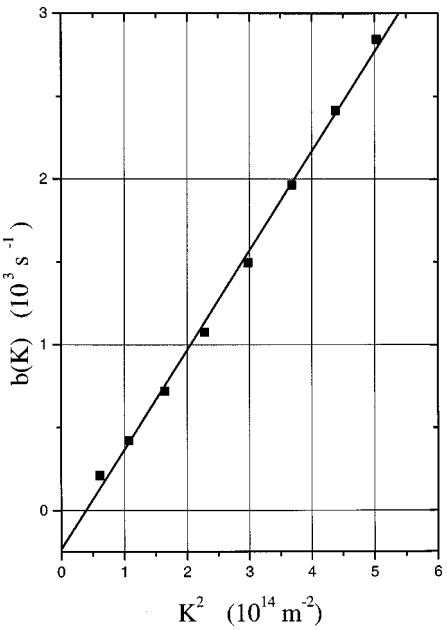

FIG. 7. The decay exponent of the intensity autocorrelation function as a function of the squared wave vector for a BACH^F sample at $\phi \approx 0.0001$. $KL = 5$ is reached for $K^2 \approx 4 \times 10^{14}$ m^{-2}. The solid line is a linear fit through the data points. From the slope the size-averaged diffusion coefficient is obtained.

B. Diffusion measurements

1. Diffusion in the limit of infinite dilution as determined with DLS

The decay exponent $b(K)$ is plotted versus the scattering vector squared K^2 in Fig. 7. The deviation from linear dependency is attributed to polydispersity: at small angles, large rods scatter most of the light contrary to larger angles. This is due to the fact that the scattering power of a single particle scales with its volume squared and, moreover, because the form factor of a small scatterer decays slower with K than of large scatterers. D_0 was obtained from a linear fit of $b(K)$ versus K^2 (see Fig. 7). In this way a size-averaged D_0 is obtained equal to 30.1×10^{-13} m^2 s^{-1}.

2. Behavior of D_s^L in the isotropic phase

Figure 8 shows that $\alpha(K)$ indeed varies linearly with K^2, which confirms that indeed long-time self-diffusion is measured. The concentration dependence of D_s^L in the isotropic phase is depicted in Fig. 9 and can be divided into three regimes. At low concentrations ($\phi < 0.008$) a linear decrease of D_s^L with increasing concentration is found. It is not certain whether the linear decrease of D_s^L really starts at $\phi = 0$ because the lowest measurable concentration was at a volume fraction of 0.003. Below this concentration the fluorescence of the samples was too low to be detected. However, by extrapolating D_s^L back to $\phi = 0$, a D_0 of 30×10^{-13} m^2 s^{-1} is found that is equal to the D_0 as determined with dynamic light scattering. This indicates that D_s^L/D_0 indeed decreases linearly at small ϕ. Although DLS and FRAP yield different size-averaged diffusion coefficients, the measurements indicate that the effect of polydispersity is not significant here. Exactly the same feature was found for colloidal silica rods

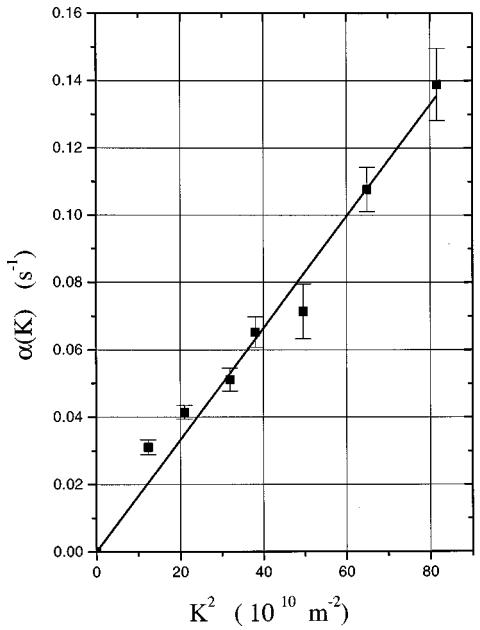

FIG. 8. The decay exponent $\alpha(K)$ of the FRAP signal as a function of the squared wave vector, measured in a sample with a volume fraction of about 1.7%. For a self diffusion process $\alpha(K)$ is proportional to K^2, with the proportionality constant equal to D_s^L.

[4]. To compare the experimentally determined D_0 with Eq. (3.2) using a solvent viscosity $\eta_m = 1.0$ mPa s for pure water at 25 °C, a length equal to $L = 261.2$ nm and a diameter $D = 13.6$ nm, we find D_0 to be 55.2×10^{-13} m^2 s^{-1}. As for the silica rods [4], we again find a theoretical single particle diffusion coefficient which is almost twice as high as experimentally determined. Polydispersity will certainly contribute to this discrepancy but the effect of an effectively higher friction due to surface irregularities may play a role as well [33]. Löwen [34] recently performed Brownian dynamics (BD) simulations on *hard* spherocylinders with aspect ratios up to 6. In this simulation only excluded volume interactions

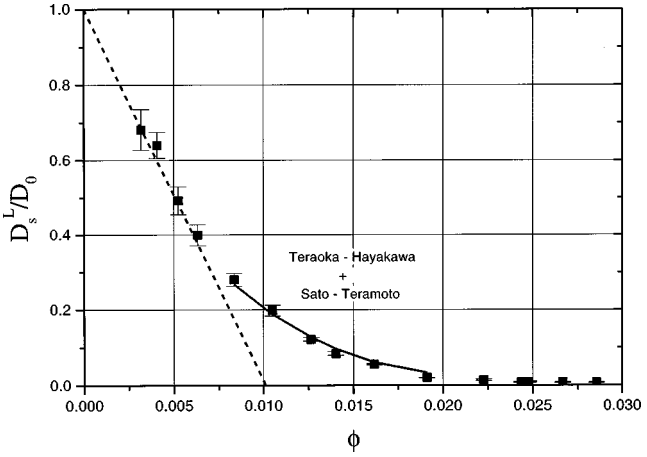

FIG. 9. The concentration dependence of the long-time self-diffusion coefficient, normalized on D_0, as a function of the volume fraction. After an initial linear dependence (the dotted line is a linear fit through the first four data points), the decrease becomes nonlinear. The solid line in this region is a fit to the prediction of the Teraoka-Hayakawa/Sato-Teramoto theory. In the biphasic region D_s^L levels and the theory fails to describe the data.

are considered and hydrodynamic interactions are neglected. Löwen gives a fit function of the concentration dependence of D_s^L/D_0 in terms of a power series of the aspect ratio and the volume fraction. The slope of D_s^L/D_0 versus the volume fraction at low concentration as found in Fig. 9 is equal to 95 ± 10. In order to compare our data with the BD simulation, the dimensions of the rods are mapped on an effective hard-core potential as demonstrated in Sec. IV A 2. The effective volume fraction can be calculated with Eq. (4.6). The slope of D_s^L/D_0 versus ϕ_{eff} then becomes 13.6 ± 1.4, whereas for an effective hard-core aspect ratio of 7.3 a slope of 5.4 is found in the BD simulations [34]. Likely, mapping the real potential onto a hard-core potential is only legitimate when $\kappa^{-1} \ll D$. For the silica rods used in Ref. [4] the condition $\kappa^{-1} \ll D$ was satisfied and a good agreement with the BD results of Löwen was found. In addition it is unclear how hydrodynamic interactions affect D_s^L in dispersions of rodlike particles interacting via long-range double-layer repulsion.

In the second regime ($0.008 < \phi < 0.019$) the concentration dependence is nonlinear. Deviation from linear dependency occurs at $D_s^L/D_0 \approx 0.4$, whereas for the silica rods [4] this point was found to be at $D_s^L/D_0 \approx 0.15$. Apparently nonlinear terms that contribute to the decrease of D_s^L are more important in this system. It is difficult to say whether this is a consequence of the fact that the rods have a larger aspect ratio or whether the long-range repulsion is responsible for this. The nonlinear regime is fitted to the Teraoka-Hayakawa/Sato-Teramoto expression given by Eq. (3.3), using $4\pi^{-1}\gamma^{-1/2}(L/D)^2$ and $4\pi^{-1}\alpha^{-1}(L/D)^2$ as the fit parameters. The factors $\frac{2}{3}\ D_{0,\perp}/D_0$ and $\frac{1}{3}\ D_{0,\parallel}/D_0$ are taken equal to $\frac{1}{2}$. Apparently the shape of Eq. (3.3) can describe our data in this region when $4\pi^{-1}\gamma^{-1/2}(L/D)^2 = 154 \pm 53$ and $4\pi^{-1}\alpha^{-1}(L/D)^2 = 49 \pm 6$. Since α is known, an ''apparent'' aspect ratio of 22 ± 3 is found that is close to the aspect ratio of the BACH rods of 19. The reason why the *hard-core* aspect ratio instead of the *effective* aspect ratio is found from this fit is explained by the fact that the rod concentration in Eq. (3.3) appears as $(L/D)^2\phi$, which quantity is not sensitive to the salt concentration when the rods are very long compared to the Debye length in the dispersion. Using this apparent aspect ratio, $\gamma^{-1/2}$ is found to be equal to 0.25. When $\phi > 0.019$ the Teraoka-Hayakawa/Sato-Teramoto expression fails to describe the data; at this volume fraction the fit displays an unphysical minimum.

In the third regime ($0.019 < \phi < 0.028$) D_s^L in the isotropic phase in coexistence with a nematic phase is reduced to roughly 1% of D_0. For a monodisperse biphasic system of rods, an increase of the overall volume fraction will lead to a linear increase of the amount of nematic phase, leaving the concentration in both coexisting phases *unchanged.* However, the system under investigation is slightly polydisperse. For a bidisperse system of rigid hard rods it has been demonstrated that the concentrations of the coexisting phases may still increase with increasing overall volume fraction [35,36]. This feature is reflected in our system by the convex increase of the amount of nematic phase with the overall volume fraction as displayed in Fig. 4, as well as by the concentration dependence of D_s^L in the coexisting isotropic phase.

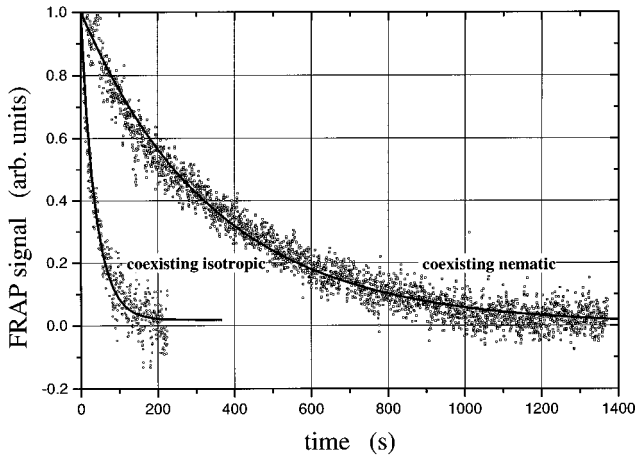

FIG. 10. The decay of the FRAP signal versus time measured in the isotropic and the coexisting nematic phase for $K^2=125\times10^{10}$ m^{-2}. In the nematic phase the FRAP geometry was adjusted such that $D_{\|}$ is monitored.

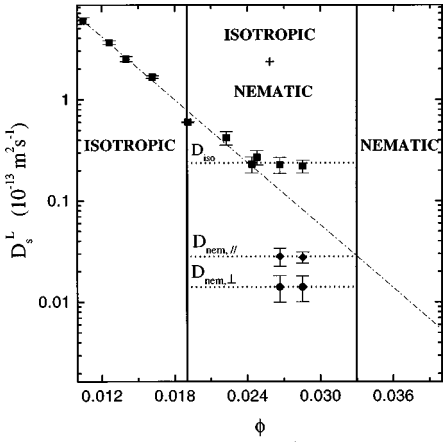

FIG. 11. The concentration dependence of D_s^L in part of the isotropic and the biphasic region in a log-linear representation. The two fat vertical lines delineate the biphasic region. In the isotropic phase (■) D_s^L decreases, even somewhat beyond ϕ_I. In the nematic phase, diffusion is about ten times slower. The dashed-dotted line is an empirical fit of the form $a10^{-b\cdot\phi}$ through part of the data in the isotropic phase (see text). Diffusion perpendicular to the long axis of the rods (●) is two times smaller than diffusion parallel to their long axis (◆).

3. Behavior of D_s^L in the nematic phase

In the nematic phase coexisting with an isotropic phase, D_s^L is roughly ten times smaller than in the coexisting isotropic phase. This is clearly shown in Fig. 10, which gives the FRAP decay curves of the isotropic and the coexisting nematic phase, both measured at the same K vector. Apparently, the fact that the nematic phase is more concentrated has a much stronger effect on the decrease of D_s^L than the gained translational freedom due to alignment of the rods. In Fig. 11 the data in the concentrated isotropic phase and the biphasic region are given in a log-linear representation. To indicate that the higher concentration in the nematic phase indeed largely affects D_s^L, the data in the isotropic phase are fitted to an empirical formula of the form $a10^{-b\cdot\phi}$, describing the data quite well when $a=72$ and $b=103$. This fit is represented by the dashed-dotted line in Fig. 11. If the isotropic phase would be quenched to $\phi=\phi_N=0.033$, this empirical formula predicts a D_s^L of 3×10^{-15} $m^2\,s^{-1}$, which is close to what is found in the *nematic* phase. The difference by a factor of 10 between both phases is therefore reasonable.

A significant change of the decay of the FRAP signal is measured when the geometry of the FRAP setup is changed. When the wave vector of the fringe pattern was made parallel to the director of the nematic, the decay is two times faster than when the wave vector is perpendicular to the director. This implies that $D_{s,\|}^L$ is two times larger than $D_{s,\perp}^L$ in the nematic phase. Note that this corresponds to the difference between $D_{0,\|}$ and $D_{0,\perp}$ for very long rods.

V. SUMMARY

A new model system of fluorescent colloidal boehmite rods was prepared and the concentration dependence of the long-time self-diffusion coefficient D_s^L was determined with FRAP. In the isotropic phase we find a concentration range where D_s^L decreases linearly with concentration. A similar extended linear regime was also found in an earlier study with silica rods [4]. Comparing the initial slope of D_s^L/D_0 versus the volume fraction with BD simulation results for hard spherocylinders [34] by mapping the potential of the boehmite rods on an effective hard-core potential did not yield satisfactory agreement; we find a much stronger concentration dependency. This may be due to the fact that mapping the dimension onto an effective hard-core is not allowed because in the current system the double-layer thickness is large compared to the diameter of the rods. For the mentioned silica rod dispersion with a relatively small Debye length, potential mapping did lead to good agreement with the BD simulations. At higher concentrations the data can be fitted by a nonlinear expression that is a combination of the theories of Sato and Teramoto [23] and Teraoka and Hayakawa [25], yielding an aspect ratio that is close to the aspect ratio of the boehmite rods. In the biphasic region, D_s^L in the isotropic phase still decreases with increasing overall volume fraction but levels before the dispersion has turned fully nematic. This is due to polydispersity of the rods resulting in volume fractions of the coexisting phases that are not entirely constant in the biphasic region. In the nematic phases long-time self-diffusion is about ten times slower than in the coexisting isotropic phase. The fact that the nematic phase is more concentrated, has a larger effect on D_s^L than the gained translational freedom due to the alignment of the rods. By spinning phase separating samples down at low speed, uniformly aligned nematics were obtained. In the ''monodomain'' nematics we were able to distinguish the sidewise self-diffusion from the lengthwise diffusion by rotating the FRAP geometry by an angle of 90°. Sidewise diffusion is two times slower than lengthwise diffusion in the nematic phase.

ACKNOWLEDGMENTS

Hoechst AG Augsburg (Germany) kindly provided the aluminum chlorohydrate. The FRAP setup is homebuilt by G. Harder. This work was supported by The Netherlands Foundation for Chemical Research (SON) with financial aid from the Netherlands Organization for Scientific Research (NWO).

[1] L. Wang, M. M. Garner, and H. Yu, Macromolecules **24**, 2368 (1991).
[2] Z. Bu, P. S. Russo, D. L. Tipton, and I. I. Negulescu, Macromolecules **27**, 6871 (1994).
[3] B. A. Scalettar, J. E. Hearst, and M. P. Klein, Macromolecules **22**, 4550 (1989).
[4] M. P. B. van Bruggen, H. N. W. Lekkerkerker, and J. K. G. Dhont, Phys. Rev. E **56**, 4394 (1997).
[5] L. Onsager, Ann. (N.Y.) Acad. Sci. **51**, 627 (1949).
[6] E. S. Wu, K. Jacobson, and D. Papahadjopoulos, Biochemistry **16**, 3936 (1977).
[7] P. F. Fahey and W. W. Webb, Biochemistry **17**, 3046 (1978).
[8] J. Käs, H. Strey, J. X. Tang, D. Finger, R. Ezzell, E. Sackmann, and P. A. Janmey, Biophys. J. **70**, 609 (1996).
[9] P. A. Buining, C. Pathmamanoharan, J. B. H. Jansen, and H. N. W. Lekkerkerker, J. Am. Ceram. Soc. **74**, 1303 (1991).
[10] M. P. B. van Bruggen, M. Donker, H. N. W. Lekkerkerker, and T. L. Hughes, Colloids Surf. (to be published).
[11] J. Y. Bottero, J. M. Cass, F. Fiessinger, and J. E. Poirier, J. Phys. Chem. **84**, 2933 (1980).
[12] J. Y. Bottero, D. Tchoubar, J. M. Cases, and F. Fiessinger, J. Phys. Chem. **86**, 3667 (1982).
[13] J. Y. Bottero, M. Axelos, D. Tchoubar, J. M. Cases, J. J. Fripiat, and F. Fiessinger, J. Colloid Interface Sci. **117**, 47 (1987).
[14] E. Matijevic, J. Colloid Interface Sci. **58**, 374 (1977).
[15] J. K. G. Dhont, *An Introduction to Dynamics of Colloids* (Elsevier, Amsterdam, 1996).
[16] F. Lanni and B. R. Ware, Rev. Sci. Instrum. **53**, 905 (1982).
[17] J. Davoust, P. F. Devaux, and L. Leger, EMBO J. **1**, 1233 (1982).
[18] A. van Blaaderen, J. Peetermans, G. Maret, and J. K. G. Dhont, J. Chem. Phys. **96**, 4591 (1992).
[19] A. Imhof, A. van Blaaderen, G. Maret, J. Mellema, and J. K. G. Dhont, J. Chem. Phys. **100**, 2170 (1994).
[20] M. M. Tirado, C. L. Martinez, and J. G. de la Torre, J. Chem. Phys. **81**, 2047 (1984).
[21] G. K. Batchelor, J. Fluid Mech. **131**, 155 (1983).
[22] B. Cichocki and B. U. Felderhof, J. Chem. Phys. **89**, 3705 (1988).
[23] T. Sato and A. Teramoto, Macromolecules **24**, 193 (1991).
[24] M. Doi and S. F. Edwards, J. Chem. Soc., Faraday Trans. 2 **74**, 560 (1978).
[25] I. Teraoka and R. Hayakawa, J. Chem. Phys. **89**, 6989 (1988).
[26] P. A. Buining, A. P. Philipse, and H. N. W. Lekkerkerker, Langmuir **10**, 2106 (1994).
[27] P. A. Buining, Y. S. J. Veldhuizen, C. Pathmamaoharan, and H. N. W. Lekkerkerker, Colloids Surface **64**, 47 (1992).
[28] A. Stroobants, H. N. W. Lekkerkerker, and T. Odijk, Macromolecules **19**, 2232 (1986).
[29] F. D. Bloss, *An Introduction to the Methods of Optical Crystallography* (Holt, Rinehart and Winston, New York, 1961).
[30] S. J. Picken, Macromolecules **23**, 464 (1990).
[31] W. A. Deer, R. A. Howie, and J. Zussman, *An Introduction to the Rock-Forming Minerals* (Longman, Harlow, 1966).
[32] A. Peterlin and H. A. Stuart, Z. Phys. **112** (1939).
[33] Van der Zande *et al.* also followed this line of reasoning to explain their smaller experimental values of D_0 found for colloidal gold rods. Results are to be published.
[34] H. Löwen, Phys. Rev. E **50**, 1232 (1994).
[35] G. J. Vroege and H. N. W. Lekkerkerker, J. Phys. Chem. **97**, 3601 (1993).
[36] P. A. Buining and H. N. W. Lekkerkerker, J. Phys. Chem. **97**, 11 510 (1993).